Influence of Disulfide Connectivity, Electrostatics, and Hydrophobicity on the Conformational Variations of α-Conotoxin GI Single-Disulfide Analogues: Simulations with Polarizable Force Field

Nan Jiang and Jing Ma*

School of Chemistry and Chemical Engineering, Institute of Theoretical and Computational Chemistry, Key Laboratory of Mesoscopic Chemistry of MOE, Nanjing University, Nanjing, 210093, People's Republic of China

Received: March 30, 2010; Revised Manuscript Received: July 16, 2010

The roles of the disulfide bridge, electrostatics, and hydrophobic/hydrophilic effects in the structural stability and conformational changes of six single-disulfide analogues of α-conotoxin GI(2−7;3−13) in aqueous solution are investigated by using molecular dynamics simulations with a fragment-based polarization model (*J. Phys. Chem. A* **2008**, *112*, 9854.). It is found that the relative stabilities are largely determined by the dipole−dipole interactions between secondary structure-based fragments, revealing the favorable effect of polar residues on conformational stabilities. The loop size closely correlates to not only the thermodynamic stability but also the local geometry of disulfide bridge. The disulfide loops with no more than five residues [GI(2−7), GI(3−7), and GI(7−13)] choose the left-handed disulfide conformation, while the larger loops [with nine and 10 residues in GI(3−13) and GI(2−13)] and a smaller disulfide loop [GI(2−3) without intercysteine residue] prefer the right-handed configuration. In the left-handed analogues, the dihedral angles concerning disulfide bonds decrease subtly along with the enlargement of disulfide loops. A converse dihedral angle and loop size relationship is found in the right-handed isomers. These results are rationalized by the strain energy of the disulfide bond as well as the electrostatic and van der Waals interactions between cysteine pairs. The single-disulfide analogues also exhibit much higher conformational diversity than the native GI. The important role of the size of hydrophobic core in the conformational evolution is also demonstrated in terms of the radius of gyration of the hydrophobic region. The radial distribution functions show the significant solvent−solute hydrogen bonding, implying that the interplay between the intermolecular and the intramolecular interactions control the dynamic process of GI single-disulfide analogues.

1. Introduction

Conotoxins have attracted extensive interest over recent years due to their therapeutic and pharmacological applications.[1−6] They are peptides isolated from the venom of cone snails, and they selectively act on a wide range of ion channels.[7−15] These peptides, which are typically 10−30 amino acid residues long, exhibit highly compact structures cross-linked by several disulfide bonds.[7−15] Among this family, α-conotoxins GI was selected as a prototype in both experimental and theoretical works. The two disulfide bonds in GI pair the first and third cysteine residues and the second and fourth cysteines, respectively.[16,17] Two conformationally constrained loops, loop I and loop II, are hence formed. The disulfide bridges play a crucial role in the structural stability and biological activity of α-conotoxin,[18−38] as well as the local geometries. Usually, the local disulfide S−S′ bond with a negative dihedral angle, $\chi_{C_\beta-S-S'-C_{\beta'}}$ (called χ in short hereafter), is named as the left-handed (LH) configuration, and a positive χ corresponds to a right-handed (RH) S−S′ bond.[39−41] For example, α-conotoxin GI has one LH Cys2−Cys7 and one RH Cys3−Cys13 disulfide bridge with $\chi = -91.8°$ and $\chi = 94.7°$, respectively, as shown in Figure 1a.[16] Quite different from GI, the disulfide bridges in other α-conotoxins, such as PnIA and PnIB, belong to the LH spiral type.[18,19] Schmidt and Hogg expanded the standard definitions of LH and RH to further consider the signs of the nearest neighboring $C_\alpha-C_\beta-S-S'$ and $S-S'-C_\beta'-C_\alpha'$ dihedral angles.[40,41] According to the statistical analysis of a large amount of NMR and X-ray protein structures, the minus LH staple (designated as −LH, having a negative $\chi_{C_\alpha-C_\beta-S-S'}$ dihedral angle) was suggested to be an allosteric configuration. However, this disulfide configuration is rare in the X-ray crystal structures due to the high strain energies with short $C_\alpha\cdots C_\alpha'$ distances.[41] In addition to the local disulfide geometry, the different disulfide pairings also affect the global configuration.[21,22] For example, both the α-conotoxin GI(2−7;3−13) and its disulfide-bonded isomer, GI(2−13;3−7), with "ribbon" connectivity CC···C···C have similar conformations.[21] In contrast, the "bead" isomer, GI(2−3;7−13), with C C···C···C connectivity, has a less globular shape.[21] Furthermore, removing one disulfide bond may result in a gross loss of secondary and tertiary structures, as well as a lack of activity.[23−38] Therefore, some simple rules to judge the effect of disulfide bridges on the local conformations and the global stability of α-conotoxin are desired.

In addition, the two disulfide bridges form a rigid hydrophobic core in the Cys2−Cys3−Asn4−Pro5−Ala6−Cys7 region, rendering the side chains of polar residues Arg9−His10−Tyr11−Ser12 exposed toward water to form a hydrophilic surface (Figure 1b). In fact, the mutations of Arg → Ala and Arg → norleucine demonstrated that the aliphatic side chains of Arg9 contributed dominantly to the affinity of GI for the muscle nAChR binding.[1] It is thus interesting to probe the interplay between the steric and the hydrophobic/hydrophilic effects on the global conformation.

* To whom correspondence should be addressed. Tel: 86-25-83597408. Fax: 86-25-83596131. E-mail: majing@nju.edu.cn.

10.1021/jp102844h
Published on Web 08/05/2010

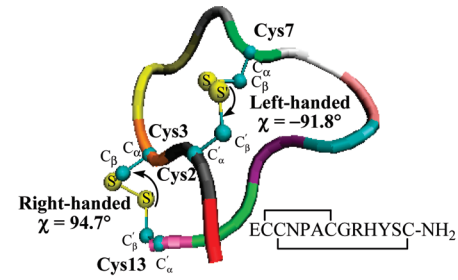

(a) Backbone structure

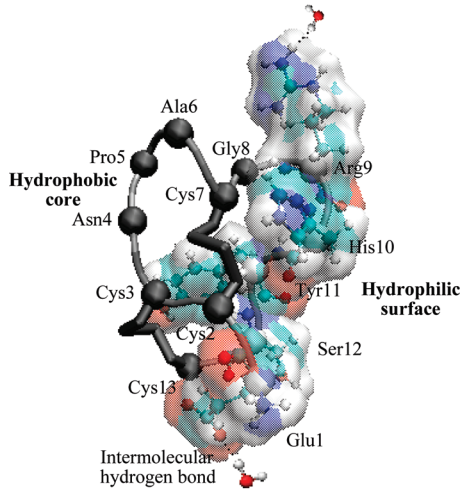

(b) The hydrophobic core and hydrophilic surface

Figure 1. (a) Amino acid sequences, backbone structure, cysteine frameworks, and disulfide bond conformations of α-conotoxin GI. The backbones and disulfide bonds are shown in the tube and CPK representations, respectively. (b) The hydrophobic core and hydrophilic surface of GI. The binary code of amino acids is adopted as follows: ○ for polar residues Arg and Glu and ● for nonpolar residues Cys, Asn, Pro, Ala, and Gly.

In the present work, we attempt to present a systematic work on the influence of the local disulfide pairing and long-range electrostatic interaction, hydrophobic core, and hydrophilic surface on the folding and conformational stability of α-conotoxin GI. Here, six single-disulfide analogues of α-conotoxin GI [GI(3−7), GI(2−7), GI(7−13), GI(2−3), GI(3−13), and GI(2−13), as shown in Figure 2] with different connectivities of disulfide bonding are selected.

Our recent theoretical work on the conformational variations of GI(2−7) and GI(3−13) in aqueous solutions has demonstrated that the molecular dynamic (MD) simulations using the FF03-based polarization model[42] can give a satisfactory description of conformational evolution. The polarizable force field is thus applied in this work to study other single-disulfide analogues in aqueous solution. The disulfide strain energy (DSE),[40,41] as well as the sum of electrostatic and van der Waals (VdW) interaction energies between cysteine pairs, correlate well with disulfide geometries. The relative stabilities of six analogues are also ranked by the polarization model and quantum mechanical (QM) calculations. The trends of relative stability of the LH and RH analogues are in line with those of the dipole−dipole interactions between polar molecular fragments, as well as those of the radius of gyration of hydrophobic cores (hydrophobic ROG) and radial distribution functions (RDFs) for the water around the hydrophilic residues. The conformational flexibility exhibits a close relationship with the loop size of disulfide bridge. The resulted structure−property relationship may add not only the clarity to protein folding but also the information to peptide libraries for pharmacological applications of conotoxins.

2. Method and Computational Details

2.1. Set-up of Initial Structures. The first model of the NMR structure of GI[17] with the Protein Data Bank[43] (PDB) code of 1XGA[21] was taken as the starting structure (the Cartesian coordinates are given in Table S1 in the Supporting Information). Six single-disulfide analogues of GI [GI(3−7), GI(2−7), GI(7−13), GI(2−3), GI(3−13), and GI(2−13)] were set up by pairing six possible single disulfide connectivities and displacing the other two cysteines by alanines (Figure S1 in the Supporting Information). These analogues were solvated in a periodic TIP3P[44] box with about 1655 water molecules. The minimum distance from the protein atom to the edge of the box was set to be about 10.0 Å. One chloride counterion was added to neutralize the charge. A cutoff radius of 12.0 Å was applied for VdW and electrostatic interactions. To move away the steric clashes, we carried out the preoptimizations before the MD simulation by using the conventional FF03 force field[45] in the Amber software.[46] Two-step energy minimizations were performed as follows: (i) 3000 steps of the steeped descent followed by 2000 conjugate gradient minimization, with a 500 kcal/mol restraint force on the protein molecule, and (ii) 10000 steps of the steeped descent followed by 2000 steps of conjugate gradient minimization without any restraints. The system was then heated slowly from 0.0 to 300.0 K over 100.0 ps with harmonic constraints on protein. Subsequently, a 1 ns conventional MD simulation was performed in the NVT ensemble with a time step of 2.0 fs.

2.2. Fragmentation-Based Polarization Model. In the traditional molecular force field, the intra- and intermolecular electrostatic interactions are often modeled by the predetermined point charges no matter how the chemical or conformational environment varies. In the fragment-based polarization model,[42] the partial charges and dipole moments are directly obtained from fragment-based QM calculations,[47−54] without the need for electrostatic parametrization. It has been demonstrated that the polarization model is able to reasonably describe the conformational variations of peptides in aqueous solutions.[42]

The potential function in the polarizable force field is expressed as follows:

$$\begin{aligned} U_{\text{total}} &= U_{\text{non-elec}} + U_{\text{elec}} \\ &= \sum_{\text{bonds}} K_b(b - b_{\text{eq}})^2 + \sum_{\text{angles}} K_\theta(\theta - \theta_{\text{eq}})^2 + \\ &\quad \sum_{\text{dihedrals}} \frac{V_n}{2}[1 + \cos(n\phi - \gamma)] + \\ &\quad \sum_{i<j} \left(\frac{A_{ij}}{R_{ij}^{12}} - \frac{B_{ij}}{R_{ij}^{6}} \right) + U_{\text{elec}} \end{aligned} \tag{1}$$

where all of the bond stretching, angle bending, torsional rotating, and Lennard−Jones parameters are taken from the FF03 force field.[45] As introduced in ref 42, the electrostatic contributions can be described by two different ways: (i) the Coulombic interactions, U_{elec}^{qq}, between atomic partial charges, q_i and q_j, as shown in eq 2

$$U_{\text{elec}}^{qq} = \sum_{i<j} k \frac{q_i q_j}{r_{ij}} \tag{2}$$

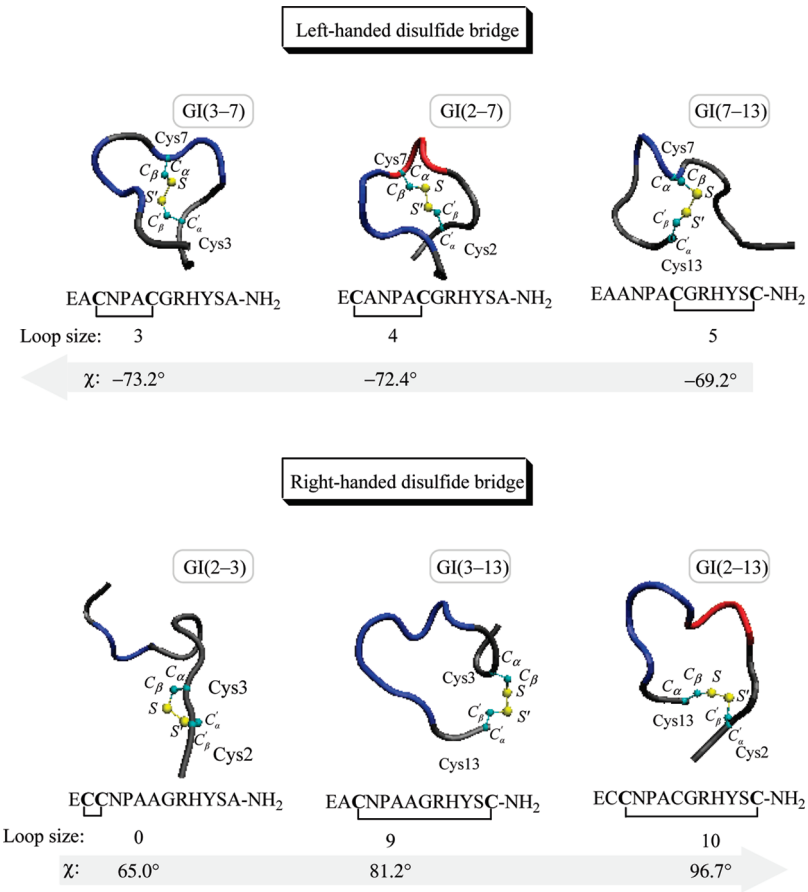

Figure 2. Amino acid sequences, backbone conformations, cysteine frameworks, and disulfide conformations of the studied single-disulfide analogues of α-conotoxin GI. These conformations are the average structures along the simulation time. NH_2 denotes an amidated C terminus. The backbones and disulfide bonds are shown in the tube and CPK representations, respectively.

or (ii) the dipole−dipole interactions, $U_{\mathrm{elec}}^{\mu\mu}$, between the fragment-centered dipole moments, μ_I^{Frag} and μ_J^{Frag}:

$$U_{\mathrm{elec}}^{\mu\mu} = \sum_{I<J} k \frac{1}{|\vec{R}_{IJ}|^3}\left(\vec{\mu}_I^{\mathrm{Frag}} \cdot \vec{\mu}_J^{\mathrm{Frag}} - 3\frac{\vec{\mu}_I^{\mathrm{Frag}} \cdot \vec{R}_{IJ} \cdot \vec{R}_{IJ} \cdot \vec{\mu}_J^{\mathrm{Frag}}}{|\vec{R}_{IJ}|^2}\right) \quad (3)$$

The electrostatic parameters of proteins and their neighboring water molecules are updated according to the environment, as shown in Figure S2 in the Supporting Information. During the molecular fragmentation calculations, we decompose the α-conotoxin GI single-disulfide analogues into fragments according to their secondary structures. For example, GI(3−7) folds into random coil in Glu1−Ala2−Cys3−Asn4 and Tyr11−Ser12−Ala13 regions. Pro5−Ala6−Cys7 and Gly8−Arg9−His10 regions exhibit a 3_{10}-helix and β-turn, respectively. Thus, we simply divide GI(3−7) into four fragments, as shown in Figure S2 in the Supporting Information. The fraction scheme can automatically vary according to the change in the secondary structure. On the basis of the fragments, a series of subsystems are constructed by capping them with their local environments. In the QM treatment of each subsystem, background point charges are introduced on the distant atoms to mimic the electrostatic interactions and polarization effect.[54−60] All of the fragmentation calculations were carried out at the B3LYP/6-31G(d) level with Gaussian03 program.[61]

2.3. Details of MD Simulations within Polarization Model. On the basis of the preoptimized structures, 3 ns MD simulations were performed within the framework of the fragmentation-based polarization model.[42] The MD simulations were run in the NPT ensemble at 300.0 K and 1.0 bar. The temperature was kept constant using the extended Langevin temperature control.[62] The pressure was maintained by using the Berendsen algorithm[63] with a coupling time $\tau_p = 1.0$ ps and compressibility $\beta_T = 4.46 \times 10^{-5}$ bar^{-1}. Bond lengths involving hydrogen atoms were kept constant by the SHAKE[64] algorithm, allowing a time step of 2.0 fs.

3. Results and Discussion

We carry out a series of MD simulations on the conformational variations of single-disulfide analogues in aqueous solutions with the typical snapshots displayed in Figure S3 in the Supporting Information. For all of the studied analogues, deleting one disulfide bridge leads to a gradual conformational change, indicating the importance of disulfide bonds in the folding and conformational stability of the proteins. The evolution of disulfide geometries (bond length $d_{S-S'}$ and dihedral angle χ) along the simulation time and the standard deviation are displayed in Figures S4 and S5 in the Supporting Information. It can be seen that the standard deviations for these disulfide geometries are comparable to each other among the studied systems. So, the geometric parameters of the average structures are employed to investigate the disulfide geometries, as shown in Figure 2 and Table 1, in which the loop sizes of the disulfide bridges are also listed. As mentioned in the Introduction, the LH and RH conformations are defined by the negative and positive values of dihedral angle χ, respectively. It can be clearly seen from Figure 2 and Table 1 that the local conformation of disulfide bridge (Cys···X_m···Cys) is closely related to the loop

TABLE 1: Loop Sizes and the Geometries (Bond Length and Dihedral Angle Are in the Units of Å and °, Respectively) of the Disulfide Bridges, as Well as the Relative Energies (kcal/mol) of the Lowest Energy Conformation of the Single-Disulfide Analogues of the α-Conotoxin GI[a]

analogues		disulfide geometries				relative energies: QM[d]		relative energies: MM[e]	
name	loop size (m)[b] (Cys···X$_m$···Cys)	χ[c]	$d_{S-S'}$	$d_{C_\alpha\cdots C_\alpha'}$	$d_{C_\beta\cdots C_\beta'}$	conventional	fragmentation	FF03-qq	FF03-$\mu\mu$
				LH disulfide bridge					
GI(3−7)	3	−73.2	2.06	6.83	3.61	33.1	35.4	24.7	37.9
GI(2−7)	4	−72.4	2.04	6.48	3.55	0.0	0.0	0.0	0.0
GI(7−13)	5	−69.2	2.03	6.07	3.50	44.6	40.1	31.0	45.4
				RH disulfide bridge					
GI(2−3)	0	65.0	2.04	4.05	3.74	46.4	40.8	57.9	68.8
GI(3−13)	9	81.2	2.05	5.47	3.91	17.1	15.0	22.7	31.6
GI(2−13)	10	96.7	2.06	5.49	3.95	13.8	12.3	16.6	27.0

[a] The relative energies are calculated from a hierarchy of theoretical approaches, fragmentation and conventional QM calculations, and the polarizable molecular mechanism (MM). [b] m is the number of amino acids X between the cysteines. [c] χ is the dihedral angle of disulfide bond, $\chi_{C_\beta-S-S'-C_\beta'}$. [d] All of the QM calculations were carried out at the B3LYP/6-31G(d) level. [e] The NBO charges were calculated in the framework of energy-based fragmentation method at the B3LYP/6-31G(d) level.

size, as indicated by the number m of residues (denoted as X) between the cysteines. The disulfide loops with three, four, and five residues choose the LH conformation. The disulfide bridges formed between the terminal cysteines (such as Cys3−Cys13 and Cys2−Cys13 with $m = 9$ and 10, respectively) or sequentially adjacent cysteines (Cys2−Cys3 with $m = 0$) favor the RH conformation.

For all of the studied analogues, we carry out two independent MD simulations starting from the LH and RH disulfide conformations, respectively. The initial LH and RH disulfide configurations are displayed in Figure S6 in the Supporting Information. The standard values of dihedral angles, $-90 \pm 30°$ and $90 \pm 30°$ for RH and LH configurations, respectively, are set for the initial configurations. The disulfide conformation evolutions from the different initial structures in all of the studied systems are shown in Figure S6 in the Supporting Information. The same disulfide configuration is converged without any conformational restraint added to the disulfides. In the case of GI(3−7), GI(2−7), and GI(7−13) analogues, both of the initial RH and LH disulfide configurations change rapidly to the LH conformations. However, for GI(2−3), GI(3−13), and GI(2−13), the RH conformation is achieved in both MD simulations with RH and LH initial configurations.

To elucidate the different conformational changes caused by the variations of disulfide pairings, we take a close look at the geometry of disulfide bond, relative stability, secondary structure, hydrophobic ROG, and electrostatics contribution from the polar residues of the left- and right-typed single-disulfide analogues, respectively. In the following subsections, we first lay emphases on the analysis of the LH single disulfide analogues and then show the similarities and differences between the LH and the RH analogues.

3.1. LH Single-Disulfide Analogues. ***3.1.1. Geometries.*** It is interesting to find from Table 1 and Figure 2 that in the single-disulfide analogues GI(3−7), GI(2−7), and GI(7−13) with LH disulfide bridge, there is a dependence of $C_\alpha\cdots C_\alpha'$ and $C_\beta\cdots C_\beta'$ distances on the size of the disulfide loops. The $C_\alpha\cdots C_\alpha'$ and $C_\beta\cdots C_\beta'$ distances decrease with the enlargement of disulfide loops from $m = 3$ to 5. The analogue GI(3−7) with $m = 3$ has the largest values of $C_\alpha\cdots C_\alpha'$ (6.83 Å) and $C_\beta\cdots C_\beta'$ distances (3.61 Å), followed by GI(2−7) with $m = 4$ ($d_{C_\alpha\cdots C_\alpha'} = 6.48$ Å, and $d_{C_\beta\cdots C_\beta'} = 3.55$ Å). GI(7−13) with the longest loop ($m = 5$) has the smallest C···C separations ($d_{C_\alpha\cdots C_\alpha'} = 6.07$ Å, and $d_{C_\beta\cdots C_\beta'} = 3.50$ Å). In the LH analogues, χ and $d_{S-S'}$ decrease gradually from −73.2° and 2.06 Å [in GI(3−7) with $m = 3$] to −69.2° and 2.03 Å [in GI(7−13) with $m = 5$]. These results may indicate that tethering the Cys7 residue to form a disulfide bridge has little influence on the local geometries.

It has been recognized that the disulfide bond configurations can be well-described in terms of the five dihedral angles, $\chi_{C-C_\alpha-C_\beta-S}$, $\chi_{C_\alpha-C_\beta-S-S'}$, $\chi_{C_\beta-S-S'-C_\beta'}$, $\chi'_{C_\alpha'-C_\beta'-S'-S}$, and $\chi'_{C'-C_\alpha'-C_\beta'-S'}$.[40,41,65−68] Accordingly, the DSE was proposed to evaluate the strain caused by the distortion of the disulfide dihedral angles.[69,70] Equation 4 gives the definition of DSE:[69,70]

$$\begin{aligned}\mathrm{DSE\ (kcal\ mol^{-1})} = \big[&8.37\big(1 + 3\cos 3\chi_{C-C_\alpha-C_\beta-S}\big) + \\ &8.37\big(1 + 3\cos 3\chi'_{C'-C_\alpha'-C_\beta'-S'}\big) + 4.18\big(1 + \cos 3\chi_{C_\alpha-C_\beta-S-S'}\big) + \\ &4.18\big(1 + \cos 3\chi'_{C_\alpha'-C_\beta'-S'-S}\big) + 14.64\big(1 + \cos 2\chi_{C_\beta-S-S'-C_\beta'}\big) + \\ &2.51\big(1 + \cos 3\chi_{C_\beta-S-S'-C_\beta'}\big)\big] \times 4.18 \quad (4)\end{aligned}$$

Although other factors such as bond lengths and VdW contacts are ignored in eq 4, this empirical formula has been demonstrated to give a semiquantitative description of the strain in a disulfide bond.[40,41,65−68]

Subsequently, we show the relationship between the DSE, obtained from eq 4, and the disulfide geometric parameter of the six single-disulfide analogues in Figure 3. It is clearly seen in Figure 3a, with the enlargement of disulfide loops from GI(3−7) to GI(7−13) (with $m = 3$ and 5, respectively), the strains in the disulfide bonds increase, along which the disulfide dihedral angles are reduced. The decrease in the $C_\alpha\cdots C_\alpha'$ distance also corresponds to the increase of DSE, as exhibited in Figure 3b.

In fact, the electrostatic interaction and steric repulsion between the cysteine pairs (as revealed from Figure 4) are responsible for the resulted disulfide geometries. The dipole−dipole interaction energies between two cysteine residues, as shown in the inset of Figure 4, indicate that electrostatic repulsion are dramatically decreased from 1039.0 to 95.5 kcal/mol as the disulfide loops increase from $m = 3$ to 5. The steric effect, reflected by VdW tension, should also be taken into account. The enhancement of VdW potential energies of cysteines pairs (such as Cys$i$ and Cys$j$) with respect to the cysteine monomers, $\Delta E_{VdW}^{int} = E_{VdW}^{Cysi\cdots Cysj} - E_{VdW}^{Cysi} - E_{VdW}^{Cysj}$, is used to characterize the steric repulsion. In contrast to the residue-based dipole−dipole interactions, the steric repulsions between cysteine pairs increase with the enlargement of loop

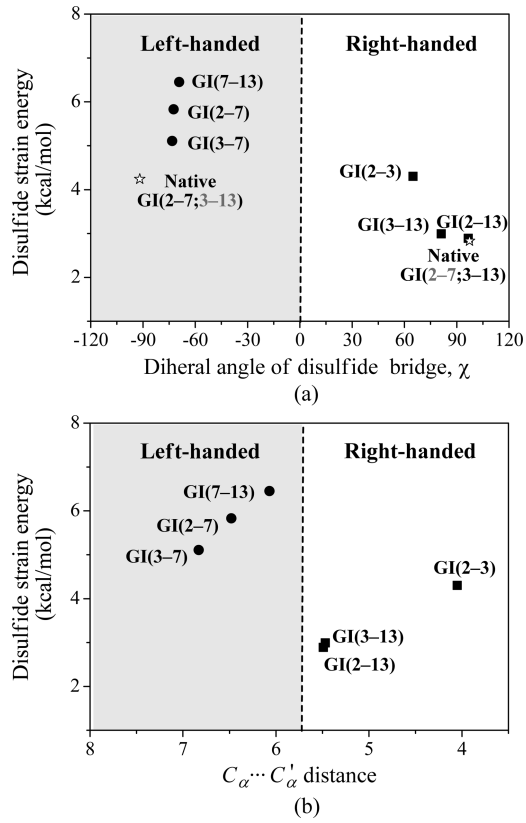

Figure 3. Correlation of the DSE with the (a) dihedral angle of disulfide bridge, χ, and (b) distance between C_α atoms.

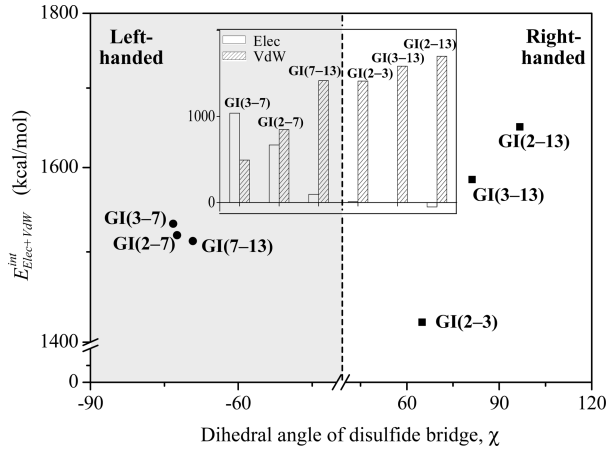

Figure 4. Correlation of the sum of electrostatic and VdW interaction energies with the dihedral angle of disulfide bridge, χ. The contributions from electrostatic (blank bargraphs) and VdW (in shadows) interaction energies concerning cysteines pairs are shown in the inset.

size. The VdW interaction energies between cysteine residues in the LH isomers ($m = 3-5$) fall in a range of 493.5−1416.9 kcal/mol. Interestingly, the sum of the repulsive electrostatic and VdW interactions exhibits a good correlation with the disulfide geometries. For example, the total nonbonding interaction follows the sequence GI(3−7) > GI(2−7) > GI(7−13), in accordance with those of the χ and disulfide distances. In addition, those nonbonding interaction energies correlate well with the calculated DSE.

3.1.2. Relative Energy of Conformers. To exploit the influence of individual disulfide connectivity on the relative stability of the studied single-disulfide isomers of α-conotoxin GI, we select the lowest energy conformers from the MD simulations to calculate their energies by a hierarchy of theoretical approaches: FF03-based polarization model,[42] fragmentation,[47−54] and conventional QM methods at the B3LYP/6-31G(d) level. Within the framework of polarization model, we use two types of force field models: (i) FF03 combined with the dynamically variable NBO charges taken from fragmentation calculations at the B3LYP/6-31G(d) level, designated as FF03-*qq*, and (ii) FF03 with fragment-centered dipole moments calculated from the NBO charges, designated as FF03-$\mu\mu$. All of the solvated water molecules are excluded in the single-point energy calculations. The results are listed in Table 1. The relative conformational stabilities of the LH single-disulfide analogues take the order GI(2−7) > GI(3−7) > GI(7−13), with *m* being 4, 3, and 5, respectively. This agrees well with the previous postulation made by Zhang and Snyder et al.[71] that the even-numbered loops have higher stability than the odd-numbered loops.

In the case of disulfide loops with odd values of *m*, there is a decrease in thermodynamic stability with the increase of disulfide loop size. The GI(3−7) with $m = 3$ is about 10 kcal/mol lower in energetics than the GI(7−13) with $m = 5$. Such a sequence of relative stability in the single-disulfide analogues will be further discussed from the view of electrostatic interactions and the dynamic variations of peptide backbones in the following subsections.

3.1.3. Electrostatic Contribution from Polar Residues. It is interesting to notice that the relative stability is largely dependent on the electrostatic interactions between the polar residues, such as Glu1 and Arg9. Table 2 presents the computational results of molecular dipole moment, $\vec{\mu}_{tot}$. It is clear that the magnitude of dipole moment decreases in the trend of GI(2−7) > GI(3−7) > GI(7−13), consistent with that of the relative thermodynamic stability. An in-depth analysis of the individual contribution from each fragment is made, with the fragment dipole moments also displayed in Table 2. Residues 1−4 and 12−13 with random coils constitute the first and fourth fragments, respectively. The second and third fragments consist of the regions of Pro5−Cys7 and Gly8−Tyr11, adopting a 3_{10}-helix and β-turn, respectively. In fragment 1, the negatively charged residue (Glu1) at the positively charged N terminus gives a net charge of zero. On the contrary, fragment 3 has a net formal charge of +1 centered on the side chain of Arg9. So, the dipole moment of the third fragment, $\vec{\mu}_3$, is significantly larger in magnitude than those of other fragments. Interestingly, the dipole moments of the third fragments among the six analogues decrease in the order GI(2−7) > GI(3−7) > GI(7−13), which is also in line with the sequence of relative energies. These results suggest the significance of the electrostatic polarization from the charged residue. The fragment-centered dipole−dipole interactions are depicted in Figure S7 in the Supporting Information. Obviously, the dipole−dipole interaction $E_{\vec{\mu}_1\vec{\mu}_3}$ between $\vec{\mu}_1$ and $\vec{\mu}_3$ is significantly larger than the others. Again, for the LH isomers, $E_{\vec{\mu}_1\vec{\mu}_3}$ exhibits the order of GI(2−7) > GI(3−7) > GI(7−13).

3.1.4. Conformational Diversity and Evolution. In addition to the relative thermodynamic stability, the dynamic behavior of single-disulfide analogues in aqueous solution is also investigated. The backbone superposition and backbone root-mean-square deviations (rmsds) are employed to investigate the conformational diversity of the single-disulfide analogues. The results are summarized in Figure 5a. In each analogue, the backbone comparison is carried out on the 10 lowest energy conformations along the trajectory of the 3 ns MD simulation. The average structure of the 10 lowest energy conformations is selected as the reference structure to calculate rmsd. To show the influence of deleting one disulfide bond on the conforma-

TABLE 2: Magnitude of Molecular Dipole Moments (Debye), $|\vec{\mu}_{tot}|$, and the Fragment-Centered Dipoles of the Six Single-Disulfide Analogues of α-Conotoxin GI at the Level of B3LYP/6-31G(d)

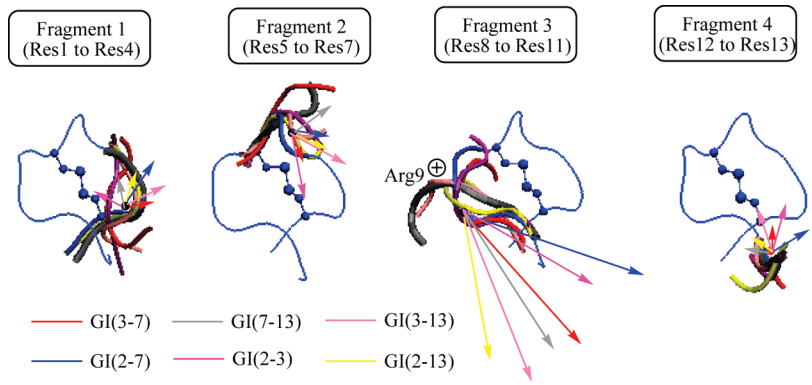

	molecular dipole	fragment dipoles			
	$\|\vec{\mu}_{tot}\|$	$\|\vec{\mu}_1\|$	$\|\vec{\mu}_2\|$	$\|\vec{\mu}_3\|$	$\|\vec{\mu}_4\|$
		LH disulfide bridge			
GI(3−7)	33.2	5.6	8.7	19.4	3.4
GI(2−7)	46.9	17.0	6.1	20.1	3.7
GI(7−13)	30.0	7.7	8.9	11.1	2.3
		RH disulfide bridge			
GI(2−3)	29.0	4.6	4.7	15.6	4.1
GI(3−13)	29.9	4.9	4.8	16.2	5.3
GI(2−13)	38.7	10.1	7.5	17.6	3.5

tional diversity, the corresponding backbone superposition and rmsd of the native double-disulfide GI(2−7;3−13) are also displayed in Figure S8 in the Supporting Information for comparison.

As displayed in Figure 5a and Figure S8a in the Supporting Information, all of the single-disulfide analogues exhibit richer conformations than the native GI(2−7;3−13). The backbone rmsds of the single-disulfide analogues are also larger than those of the native one. This indicates that removing one disulfide bond leads to higher flexibility and hence a collapse in the native compact conformation.

In addition, the backbone rmsd shows that the diversity of the LH analogues increases in the order of GI(2−7) < GI(3−7) < GI(7−13). In addition, the alternation of disulfide connectivity leads to a very different structure and, consequently, results in the different exposed surfaces in aqueous solution. The isomers with LH disulfide bridges have the near-globular surface, with a decreasing degree of sphericity, GI(2−7) > GI(3−7) > GI(7−13), as shown in Figure 6.

The time evolutions of secondary structure for each residue of the LH single-disulfide analogues are shown in Figure 5b. For the purpose of comparison, the variation of secondary

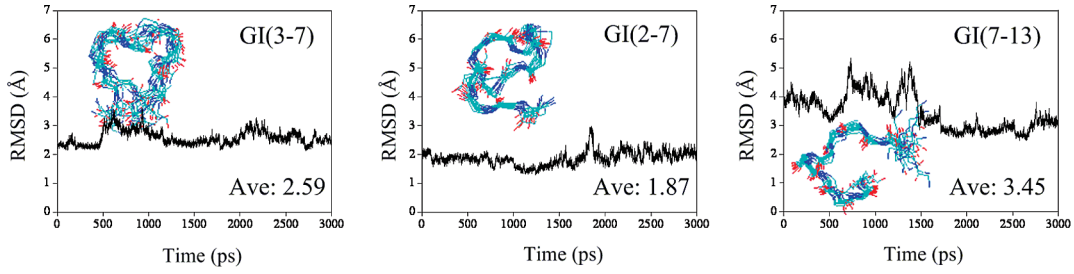

(a) Backbone RMSD and conformational superposition

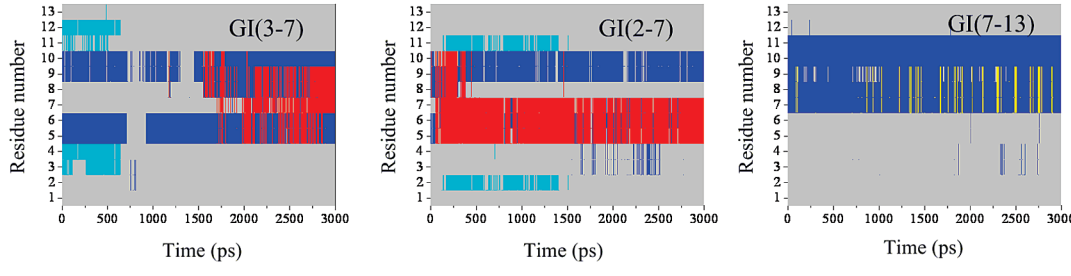

(b) Time evolution of the secondary structures

Figure 5. Time evolution of (a) backbone atom rmsds and (b) the secondary structures of the single-disulfide analogues of α-conotoxin GI with LH disulfide bridges in 3 ns MD simulations with a polarizable FF03-*qq* model (NPT ensemble at 300.0 K and 1.0 bar). The rmsds are calculated with the average structure of the 10 lowest energy conformations taken as the reference structure.

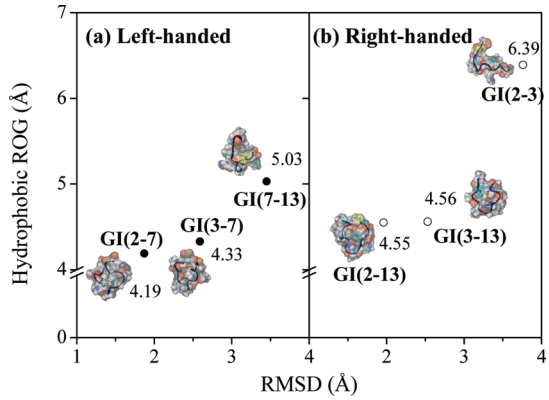

Figure 6. Correlation between the ROG of hydrophobic cores and backbone rmsd in the single-disulfide analogues of α-conotoxin GI.

structures of α-conotoxin GI along the simulation time is also exhibited in Figure S8b in the Supporting Information. There are two distinct helical regions in the native GI(2−7;3−13), α-helix and β-turn, which are shown by yellow and blue regions, respectively. With the loss of one disulfide bridge, these helical regions are converted to other secondary structures such as a 3_{10}-helix (red), β-turn (blue), and random coil (gray).

The conformational evolution process can also be visualized from the change in the population of secondary structures. The results are displayed in Figure S9 in the Supporting Information. With respect to GI(2−7), the 3_{10}-helix in the Pro5−Cys7 region is gradually replaced by a β-turn and random coil in GI(3−7) and GI(7−13), respectively. The sum of the population of the 3_{10}-helix and β-turn decreases in the order of GI(2−7) (49%) > GI(3−7) (38%) > GI(7−13) (31%), in line with the trend of relative thermodynamic stability among the LH analogues.

The important role of hydrophobic core in conformational conversion can be understood by variations in the hydrophobic ROG, which is defined as[72]

$$\mathrm{Rg} = \left(\frac{\sum_i ||r_i||^2 m_i}{\sum_i m_i} \right)^{1/2} \quad (5)$$

where m_i is the mass of atom i and r_i is the position of atom i with respect to the center of mass of the hydrophobic core. As displayed in Figure 6, the calculated hydrophobic ROG values follow the sequence GI(2−7) < GI(3−7) < GI(7−13), with the values of 4.19, 4.33, and 5.03 Å, respectively. This agrees well with the relative compactness of the 3_{10}-helix, β-turn, and random coil. Among these configurations, the 3_{10}-helix and β-turn are stabilized by i, $i + 3$ and i, $i + 4$ intramolecular hydrogen bonding, respectively. In addition, the average values of backbone rmsds of LH single-disulfide analogues are correlated well with the ROG values, as shown in Figure 6.

3.2. Comparisons between RH and LH Analogues. ***3.2.1. Similarities.*** The RH single-disulfide analogues share some similarities with the LH isomers. (i) In the case of the RH single-disulfide analogues, positive charges on the side chain of Arg9 also make the magnitude of dipole moments of the third fragments significantly larger than those of other fragments (Table 2). The dipole−dipole interactions between fragments with charge centers also dominate the relative stabilities, as shown in Figure S7 in the Supporting Information. Consequently, the relative stability shares the same sequence with the dipole−dipole interactions: GI(2−13) > GI(3−13) > GI(2−3).

(ii) Deletion of a disulfide bridge also results in the dynamic variations for the RH analogues in aqueous solutions. According to the rmsd variations in Figure 7 and Figure S8 in the Supporting Information, the RH single-disulfide isomers, exhibiting much richer conformations in aqueous solution, are found to be more flexible than the native GI(2−7;3−13). The MD simulations show that the conformation of RH analogue changes gradually in aqueous solutions (Figure S3 in the Supporting Information). In addition, the time evolutions of secondary structure for each residue of single-disulfide analogues with RH spiral conformation are also shown in Figure 7b. The 3_{10}-helix in Pro5−Cys7 dominates in GI(3−13) and GI(2−13).

(iii) The dynamics of the RH single-disulfide analogues also bears a close relationship with the thermodynamic stability. As displayed in Figure S9 in the Supporting Information, the sum of 3_{10}-helix and β-turn populations follows the order GI(2−13) (38%) > GI(3−13) (22%) > GI(2−3) (14%), which is the same as that of the conformational stability. Furthermore, as displayed in Figure 6, the relative order of the backbone rmsd values for the RH isomers agrees well with that of the ROG of hydrophobic cores [6.39 Å in GI(2−3), 4.56 Å in GI(3−13), and 4.55 Å in GI(2−13), respectively].

3.2.2. Differences. Despite the similarities, there are several differences between the RH and the LH single-disulfide analogues. These differences lie in the correlation of disulfide bond geometries and conformational stabilities with the loop size of disulfide bridges.

(i) In comparison with the LH analogues, the $C_\alpha \cdots C_\alpha'$ distance in the RH analogues is shorter. The calculated average value of $C_\alpha \cdots C_\alpha'$ distances among all of the studied single-disulfide analogues is 5.73 Å, close to the mean value of 5.64 Å on the basis of the statistical analysis of a large number of protein structures.[40]

On the other hand, in contrast to the analogues with LH disulfide bridges, the dihedral angles, χ, and bond lengths, $d_{S-S'}$, of disulfide bonds in the RH isomers [GI(2−3), GI(3−13), and GI(2−13)] are increased with the enlargement of disulfide loops. $C_\alpha \cdots C_\alpha'$ and $C_\beta \cdots C_\beta'$ distances also become larger as the disulfide loops are longer. These disulfide geometries show a good correlation with DSE. As shown in Figure 3a,b, as the dihedral angle χ and $C_\alpha \cdots C_\alpha'$ distance increase from GI(2−3) to GI(2−13), the DSE shows a decreasing tendency. In contrast to the electrostatic repulsion (9.6 kcal/mol) between the cysteine pair in GI(2−3), the tether of two termini by disulfide bond leads to electrostatic attraction with interaction energies of about −50.2 kcal/mol in GI(2−13) (Figure 4). However, it is interesting to find in Figure 4 that the steric repulsions (in the range of 1411.9−1650.3 kcal/mol) are much larger than the electrostatic interactions, so that the VdW interactions between Cys−Cys pairs dominate the sum of nonbonded VdW and electrostatic interactions. The trend of GI(2−13) > GI(3−13) > GI(2−3) in steric repulsion (shown in Figure 4) correlates well with the disulfide loop size m (i.e., 10, 9, and 0, respectively).

(ii) Although the dependence of the odd−even property of m cannot be directly applied to judge the relative stability of RH isomers, the loop size is one of the most important factors determining the relative thermodynamic stability of the RH isomers. As shown in Table 1, the relative conformational energies obtained from both the polarization model and the quantum chemistry calculations take a decreasing order of GI(2−3) > GI(3−13) > GI(2−13). This sequence reflects that as the loop sizes become larger, the thermodynamic stabilities increase. Furthermore, in the RH single-disulfide analogues,

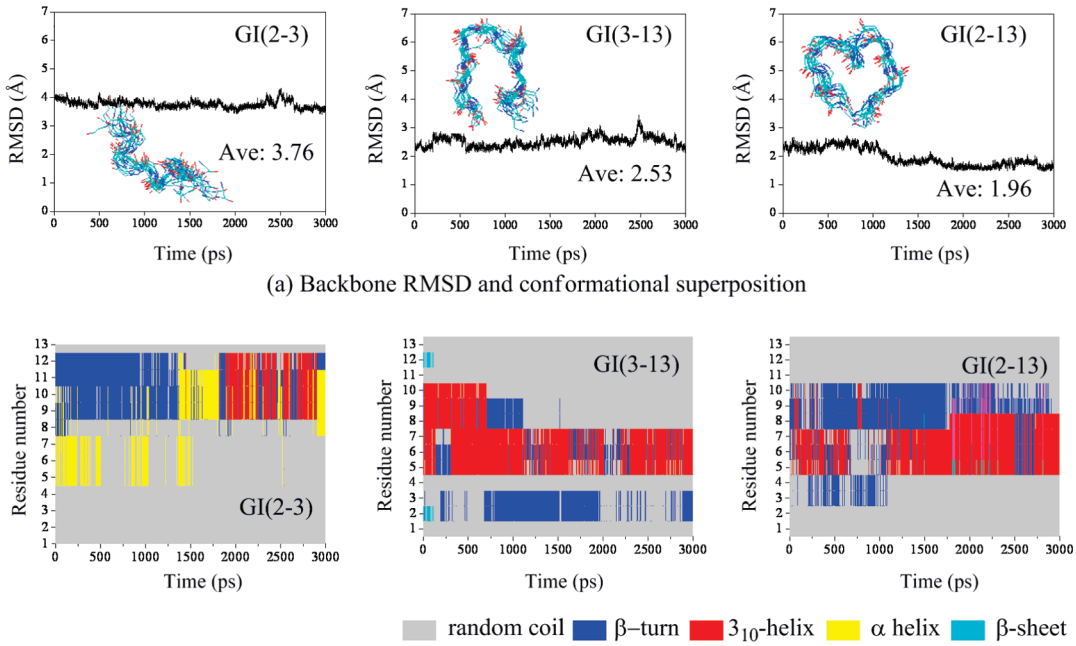

Figure 7. Time evolution of (a) backbone atom rmsds and (b) the secondary structures of the single-disulfide analogues of α-conotoxin GI with RH disulfide bridges in 3 ns MD simulations with a polarizable FF03-*qq* model (NPT ensemble at 300.0 K and 1.0 bar). The rmsds are calculated with the average structure of the 10 lowest energy conformations taken as the reference structure.

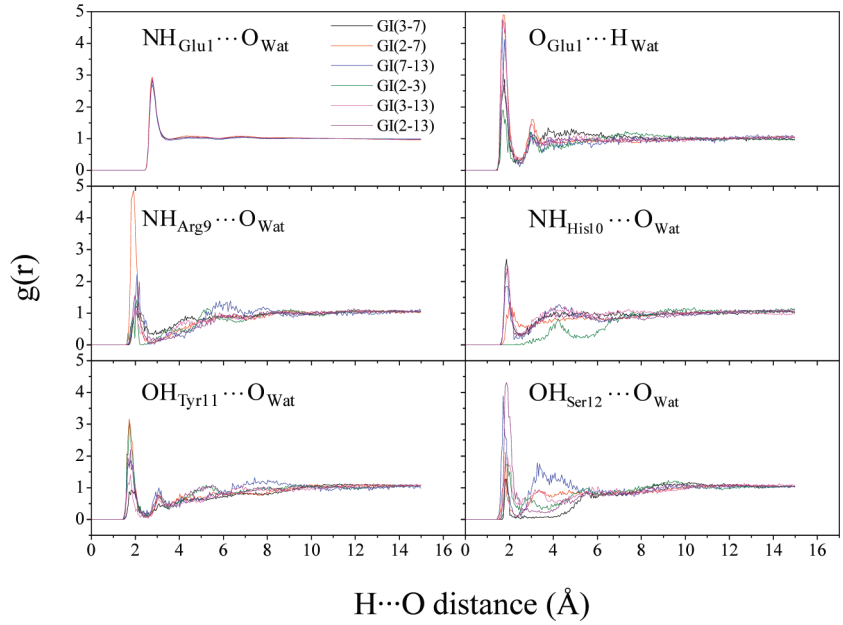

Figure 8. RDF for the water around the hydrophilic residues in the single-disulfide analogues of α-conotoxin.

there is also an apparent correlation of conformational flexibility with the size of disulfide loops. As the disulfide loops are enlarged, the increase of flexibility goes from GI(2−13) and GI(3−13) to GI(2−3), with the average backbone rmsds of 1.96, 2.53, and 3.76 Å, respectively (Figure 7a). The high flexibility of GI(2−3) is also manifested by a multitude of conformers in solution.

From the above discussion, it can be seen that the conformations of GI(2−7) and GI(3−13), which retain one pairing of the disulfide bonds in the natural GI(2−7;3−13), do not change much in the course of the simulation. It implies that the GI(2−7) and GI(3−13) analogues conserve the geometry of the native GI(2−7;3−13) to a large degree. Therefore, the 2−7 and 3−13 pairings are the most import combinations among the various possible disulfide connectivities.

3.3. Intermolecular Hydrogen Bonding in Aqueous Solution. As mentioned above, the electrostatic interactions between the polar residues, especially those with charges centered on side chains, stabilize the single-disulfide analogues. This also suggests the significant intermolecular interactions between the polar residues and the solvent. We focus on the intermolecular hydrogen-bonding interactions between the water and the N-terminal glutamic acid residue (Glu1) and the side chains of the hydrophilic residues, Arg9, His10, Tyr11, and Ser12. The solvation sphere around the peptide is described by using RDF. As expected, there exist strong interactions between the central O (or H) atoms of peptides and the water H (or O). As shown in Figure 8, the average distances of $R_{O\cdots H}$ are located at about 2.01 Å. Obviously, the significant hydrogen bonding between

water molecules and hydrophilic residues Arg9, His10, and Tyr11 is originated from the large dipole moment of the third fragment.

It is interesting to investigate the relationship between the intermolecular hydrogen bonding and the relative thermodynamic stability or the conformational variations of the six analogues. As displayed in Figure 8, there are many intermolecular hydrogen-bonding interactions between the single-disulfide analogues and the water molecules, such as $NH_{Glu1}\cdots O_{Wat}$, $O_{Glu1}\cdots H_{Wat}$, $OH_{His10}\cdots O_{Wat}$, and so on. The cooperative effect among these hydrogen bonds makes it is difficult to pick out a single H···O contribution to the relative thermodynamic stability. So, we survey the average solute−solvent H···O distance and the coordination number of water molecules around the solute, with the results shown in Table S2 in the Supporting Information. The H···O distances fall into a range of 1.96−1.99 Å. The coordination number decreases from 3.6 to 1.8, correlating well with the relative energies GI(2−3) > GI(7−13) > GI(3−7) > GI(3−13) > GI(2−13) > GI(2−7). The difference in the coordination number of water molecules around the single-disulfide analogues results from the different shapes of the exposed surfaces and the size of hydrophobic cores. As shown in Figure S10 in the Supporting Information, GI(2−7) and GI(3−7) with the near-globular surface have relatively larger coordination numbers of water of about 3.6 and 2.8, respectively. However, the analogue of GI(2−3) with a ribbonlike surface contains the least coordinated water molecules of about 1.8. In addition, the relationship between the coordination number of water molecules and the hydrophobic ROG of the studied systems is also displayed in Figure S10 in the Supporting Information. The capability of hosting more coordinated water molecules is correlated with the compactness of hydrophobic core. In conclusion, the interplay between the intermolecular solvent−solute hydrogen bonding and the intramolecular interactions in peptide controls the conformational variations of single-disulfide analogues of α-conotoxin GI in aqueous solution.

4. Conclusion

The relative thermodynamic stabilities and conformational variations of the six single-disulfide analogues of the α-conotoxin GI(2−7;3−13) in aqueous solutions have been investigated by MD simulations with a polarizable force field. It has been demonstrated that the dipole−dipole interactions between polar residues govern the relative stabilities of the single-disulfide analogues. In addition, the properties of local motifs, such as the loop size and odd−even property of the number of amino acids between the cysteines, are important factors in understanding the sequence in relative conformational stability and local geometry of disulfide bonds. The disulfide bridges with no more than five residues in the disulfide loops [GI(2−7, GI(3−7), and GI(7−13)] prefer the LH conformation, while the larger [GI(3−13) and GI(2−13)] or smaller loops [GI(2−3)] choose the RH conformation. Both the DSE and the sum of dipole−dipole and van der Waal interactions between cysteine pairs are closely related to the conformations of single-disulfide analogues.

Deletion of one disulfide bridge in the α-conotoxin GI leads to evident conformational variations of the single-disulfide analogues in aqueous solutions. The helical regions change into other secondary structures, such as a 3_{10}-helix, β-turn, and random coil. When the single-disulfide analogues exhibit much richer conformations, the ROG values of hydrophobic cores also increase, indicating the important role of the size of hydrophobic core in the conformational evolution. The significant intermolecular N−H···O and O···H−O hydrogen-bonding interactions between the solvent molecules and the hydrophilic residues are also shown to affect the conformational variations of single-disulfide analogues in aqueous solution. These results may be helpful for providing information on protein folding and potential applications in drug design.

Acknowledgment. This work was supported by the National Natural Science Foundation of China (No. 20825312), National Basic Research Program (Grant No. 2004CB719901), and the Fok Ying Tong Education Foundation (Grant No. 111013), the Ministry of Science and Technology of China for the International Science Linkages Program (2009DFA50620).

Supporting Information Available: Initial structures of the six single-disulfide analogues (Figure S1); fragmentation scheme and variation in partial charges on atoms during MD simulations (Figure S2); MD snapshots of single-disulfide analogues in the polarization model (Figure S3); time evolution of dihedral angles (Figure S4) and bond length (Figure S5); evolution of disulfide configurations of the six single-disulfide analogues starting with LH and RH disulfide bridges, respectively (Figure S6); fragment-based dipole−dipole interaction energies (Figure S7); backbone rmsd and secondary structure evolutions for the native α-conotoxin GI (Figure S8); population of the most probable secondary structure per residue (Figure S9); correlation between the number of the coordinated water molecules and the hydrophobic ROG (Figure S10); Carstesian coordinates of the first model of the NMR structure of GI with the PDB code of 1XGA (Table S1); and solute−solvent hydrogen-bonding length and the coordination number of water around solute (Table S2). This material is available free of charge via the Internet at http://pubs.acs.org.

References and Notes

(1) Groebe, D. R.; Gray, W. R.; Abramson, S. N. *Biochemistry* **1997**, *36*, 6469.
(2) Milganich, G. P.; Ramachandran, J. *Annu. Rev. Pharmacol. Toxicol.* **1995**, *35*, 707.
(3) Sabatier, J. M.; Lecomte, C.; Mabrouk, K.; Darbon, H.; Oughideni, R.; Canarelli, S.; Rochat, H.; Martin-Eauclaire, M. F.; Van Rietschoten, J. *Biochemistry* **1996**, *35*, 10641.
(4) Hu, S. H.; Loughnan, M.; Miller, R.; Weeks, C. M.; Blessing, R. H.; Alewood, P. F.; Lewis, R. J.; Martin, J. L. *Biochemistry* **1998**, *37*, 11425.
(5) Song, J.; Gilquin, B.; Jamin, N.; Drakopoulou, E.; Guenneugues, M.; Dauplais, M.; Vita, C.; Ménez, A. *Biochemistry* **1997**, *36*, 3760.
(6) Pent, C.; Han, Y.; Sanders, T.; Chew, G.; Liu, J.; Hawrot, E.; Chi, C.; Wang, C. *Peptides* **2008**, *29*, 1700.
(7) Martinez, J. S.; Olivera, B. M.; Gray, W. R.; Craig, A. G.; Groebe, D. R.; Abramson, S. N.; McIntosh, J. M. *Biochemistry* **1995**, *34*, 14519.
(8) Cartier, G. E.; Yoshikami, D.; Gray, W. R.; Luo, S.; Olivera, B. M.; McIntosh, J. M. *J. Biol. Chem.* **1996**, *271*, 7522.
(9) Gouda, H.; Yamazaki, K. I.; Hasegawa, J.; Kobayashi, Y.; Nishiuchi, Y.; Sakakibara, S.; Hirono, S. *Biochim. Biophys. Acta* **1997**, *1343*, 327.
(10) Quiram, P. A.; Sine, S. M. *J. Biol. Chem.* **1998**, *273*, 11007.
(11) Favreau, P.; Krimm, I.; Gall, F. L.; Bobenrieth, M. J.; Lamthanh, H.; Bouet, F.; Servent, D.; Molgo, J.; Ménez, A.; Letourneux, Y.; Lancelin, J. M. *Biochemistry* **1999**, *38*, 6317.
(12) Gehrmann, J.; Daly, N. L.; Alewood, P. F.; Craik, D. J. *J. Med. Chem.* **1999**, *42*, 2364.
(13) Mok, K. H.; Han, K. H. *Biochemistry* **1999**, *38*, 11895.
(14) Jacobsen, R. B.; DelaCruz, R. G.; Grose, J. H.; McIntosh, J. M.; Yoshikami, D.; Olivera, B. M. *Biochemistry* **1999**, *38*, 13310.
(15) Kang, T. S.; Vivekanandan, S.; Jois, S. D. S.; Kini, R. M. *Angew. Chem., Int. Ed.* **2005**, *44*, 6333.
(16) Guddat, L. W.; Martin, J. A.; Shan, L.; Edmundson, A. B.; Gray, W. R. *Biochemistry* **1996**, *35*, 11329.
(17) Pardi, A.; Galdes, A.; Florance, J.; Maniconte, D. *Biochemistry* **1989**, *28*, 5494.
(18) Hu, S. H.; Gehrmann, J.; Guddat, L. W.; Alewood, P. F.; Craik, D. J.; Martin, J. L. *Structure* **1996**, *4*, 417.

(19) Hu, S. H.; Gehrmann, J.; Alewood, P. F.; Craik, D. J.; Martin, J. L. *Biochemistry* **1997**, *36*, 11323.
(20) Kang, T. S.; Radić, Z.; Talley, T. T.; Jois, S. D. S.; Taylor, P.; Kini, R. M. *Biochemistry* **2007**, *46*, 3338.
(21) Gehrmann, J.; Alewood, P. F.; Craik, D. J. *J. Mol. Biol.* **1998**, *278*, 401.
(22) Lovelace, E. S.; Armishaw, C. J.; Colgrave, M. L.; Wahlstrom, M. E.; Alewood, P. F.; Daly, N. L.; Craik, D. J. *J. Med. Chem.* **2006**, *49*, 6561.
(23) Kaerner, A.; Rabenstein, D. L. *Biochemistry* **1999**, *38*, 5459.
(24) Van Mierlo, C. P.; Darby, N. J.; Neuhaus, D.; Creighton, T. E. *J. Mol. Biol.* **1991**, *222*, 353.
(25) Rabenstein, D. L.; Yeo, P. L. *J. Org. Chem.* **1994**, *59*, 4223.
(26) Rabenstein, D. L.; Weaver, K. H. *J. Org. Chem.* **1996**, *61*, 7391.
(27) Hua, Q. X.; Narhi, L.; Jia, W.; Arakawa, T.; Rosenfeld, R.; Hawkins, N.; Miller, J. A.; Weiss, M. A. *J. Mol. Biol.* **1996**, *259*, 297.
(28) Price-Carter, M.; Gray, W. R.; Goldenberg, D. P. *Biochemistry* **1996**, *35*, 15537.
(29) Price-Carter, M.; Gray, W. R.; Goldenberg, D. P. *Biochemistry* **1996**, *35*, 15547.
(30) Laity, J. H.; Lester, C. C.; Shimotakahara, S.; Zimmerman, D. E.; Montelione, G. T.; Scheraga, H. A. *Biochemistry* **1997**, *36*, 12683.
(31) Shimotakahara, S.; Ríos, C. B.; Laity, J. H.; Zimmerman, D. E.; Scheraga, H. A.; Montelione, G. T. *Biochemistry* **1997**, *36*, 6915.
(32) Barnham, K. J.; Torres, A. M.; Alewood, D.; Alewood, P. F.; Domagala, T.; Nice, E. C.; Norton, R. S. *Protein Sci.* **1998**, *7*, 1738.
(33) Flinn, J. P.; Pallaghy, P. K.; Lew, M. J.; Murphy, R.; Angus, J. A.; Norton, R. S. *Biochim. Biophys. Acta* **1999**, *1434*, 177.
(34) Price-Carter, M.; Hull, M. S.; Goldenberg, D. P. *Biochemistry* **1998**, *37*, 9851.
(35) Chuang, L. C.; Chen, P. Y.; Chen, C.; Huang, T. H.; Wang, K. T.; Chiou, S. H.; Wu, S. H. *Biochem. Biophys. Res. Commun.* **1996**, *220*, 246.
(36) Ota, M.; Shimizu, Y.; Tonosaki, K.; Ariyoshi, Y. *Biopolymers* **1998**, *46*, 65.
(37) Pace, C. N.; Grimsley, G. R.; Thomson, J. A.; Barnett, B. J. *J. Biol. Chem.* **1988**, *263*, 11820.
(38) Zhang, R.; Snyder, G. H. *Biochemistry* **1991**, *30*, 11343.
(39) Richardson, J. S.; Richardson, D. C. In *Prediction of Protein Structure and the Principles of Protein Conformation*; Fasman, G. D., Ed.; Plenum Press.: New York, 1989; pp 1−99.
(40) Schmidt, B.; Hogg, P. J. *BMC Struct. Biol.* **2007**, *7*, 49.
(41) Schmidt, B.; Ho, L.; Hogg, P. J. *Biochemistry* **2006**, *45*, 7429.
(42) Jiang, N.; Ma, J. *J. Phys. Chem. A* **2008**, *112*, 9854.
(43) Berman, H. M.; Westbrook, J.; Feng, Z.; Gilliland, G.; Bhat, T. N.; Weissig, H.; Shindyalov, I. N.; Bourne, P. E. *Nucleic Acid Res.* **2000**, *28*, 235.
(44) Jorgensen, W. L.; Chandrasekhar, J.; Madura, J. D.; Klein, M. L. *J. Chem. Phys.* **1983**, *79*, 926.
(45) Duan, Y.; Wu, C.; Chowdhury, S.; Lee, M. C.; Xiong, G.; Zhang, W.; Yang, R.; Cieplak, P.; Luo, R.; Lee, T.; Caldwell, J.; Wang, J.; Kollman, P. *J. Comput. Chem.* **2003**, *24*, 1999.
(46) Case, D. A.; Darden, T. A.; Cheatham, T. E., III; Simmerling, C. L.; Wang, J.; Duke, R. E.; Luo, R.; Merz, K. M.; Pearlman, D. A.; Crowley, M.; Walker, R. C.; Zhang, W.; Wang, B.; Hayik, S.; Roitberg, A.; Seabra, G.; Wong, K. F.; Paesani, F.; Wu, X.; Brozell, S.; Tsui, V.; Gohlke, H.; Yang, L.; Tan, C.; Mongan, J.; Hornak, V.; Cui, G.; Beroza, P.; Mathews, D. H.; Schafmeister, C.; Ross, W. S.; Kollman, P. A. *AMBER 9*; University of California: San Francisco, 2006.
(47) Li, S.; Li, W.; Fang, T.; Ma, J.; Jiang, Y. *Low Scaling Quantum Chemical (LSQC) Program*, version 1.1; Nanjing University: Nanjing, 2006.
(48) Li, S.; Li, W.; Fang, T. *J. Am. Chem. Soc.* **2005**, *127*, 7215.
(49) Li, W.; Fang, T.; Li, S. *J. Chem. Phys.* **2006**, *124*, 154102.
(50) Li, W.; Li, S.; Jiang, Y. *J. Phys. Chem. A* **2007**, *111*, 2193.
(51) Li, S.; Li, W. *Annu. Rep. Prog. Chem., Sect. C: Phys. Chem.* **2008**, *104*, 256.
(52) Li, W.; Dong, H.; Li, S. *Relative Energies of Proteins and Water Clusters Predicted with Generalized Energy-Based Fragmentation Approach. Frontiers in Quantum Systems in Chemistry and Physics*; Springer: Netherlands, 2008; p 289.
(53) Hua, W.; Fang, T.; Li, W.; Yu, J. G.; Li, S. *J. Phys. Chem. A* **2008**, *112*, 10864.
(54) Jiang, N.; Ma, J.; Jiang, Y. *J. Chem. Phys.* **2006**, *124*, 114112.
(55) Morita, S.; Sakai, S. *J. Comput. Chem.* **2001**, *22*, 1107.
(56) Exner, T. E.; Mezey, P. G. *J. Phys. Chem. A* **2004**, *108*, 4301.
(57) Sakai, S.; Morita, S. *J. Phys. Chem. A* **2005**, *109*, 8424.
(58) Dahlke, E. E.; Truhlar, D. G. *J. Chem. Theory Comput.* **2007**, *3*, 46.
(59) Dahlke, E. E.; Truhlar, D. G. *J. Chem. Theory Comput.* **2008**, *4*, 1.
(60) Dahlke, E. E.; Leverentz, H. R.; Truhlar, D. G. *J. Chem. Theory Comput.* **2008**, *4*, 33.
(61) Frisch, M. J.; Trucks, G. W.; Schlegel, H. B.; Scuseria, G. E.; Robb, M. A.; Cheeseman, J. R.; Montgomery, J. A., Jr.; Vreven, T.; Kudin, K. N.; Burant, J. C.; Millam, J. M.; Iyengar, S. S.; Tomasi, J.; Barone, V.; Mennucci, B.; Cossi, M.; Scalmani, G.; Rega, N.; Petersson, G. A.; Nakatsuji, H.; Hada, M.; Ehara, M.; Toyota, K.; Fukuda, R.; Hasegawa, J.; Ishida, M.; Nakajima, T.; Honda, Y.; Kitao, O.; Nakai, H.; Klene, M.; Li, X.; Knox, J. E.; Hratchian, H. P.; Cross, J. B.; Bakken, V.; Adamo, C.; Jaramillo, J.; Gomperts, R.; Stratmann, R. E.; Yazyev, O.; Austin, A. J.; Cammi, R.; Pomelli, C.; Ochterski, J. W.; Ayala, P. Y.; Morokuma, K.; Voth, G. A.; Salvador, P.; Dannenberg, J. J.; Zakrzewski, V. G.; Dapprich, S.; Daniels, A. D.; Strain, M. C.; Farkas, O.; Malick, D. K.; Rabuck, A. D.; Raghavachari, K.; Foresman, J. B.; Ortiz, J. V.; Cui, Q.; Baboul, A. G.; Clifford, S.; Cioslowski, J.; Stefanov, B. B.; Liu, G.; Liashenko, A.; Piskorz, P.; Komaromi, I.; Martin, R. L.; Fox, D. J.; Keith, T.; Al-Laham, M. A.; Peng, C. Y.; Nanayakkara, A.; Challacombe, M.; Gill, P. M. W.; Johnson, B.; Chen, W.; Wong, M. W.; Gonzalez, C.; Pople, J. A. *Gaussian 03*, revision D.01; Gaussian, Inc.: Wallingford, CT, 2003.
(62) Wu, X.; Brooks, B. R. *Chem. Phys. Lett.* **2003**, *381*, 512.
(63) Berendsen, H. J. C.; Postma, J. P. M.; Van Gunsteren, W. F.; Di Nola, A.; Haak, J. R. *J. Chem. Phys.* **1984**, *81*, 3684.
(64) Ryckaert, J. P.; Ciccotti, G.; Berendsen, H. J. C. *J. Comput. Phys.* **1977**, *23*, 327.
(65) Wells, J. A.; Powers, D. B. *J. Biol. Chem.* **1986**, *261*, 6564.
(66) Kuwajima, K.; Ikeguchi, M.; Sugawara, T.; Hiraoka, Y.; Sugai, S. *Biochemistry* **1990**, *29*, 8240.
(67) Wetzel, R.; Perry, L. J.; Baase, W. A.; Becktel, W. J. *Proc. Natl. Acad. Sci. U.S.A.* **1988**, *85*, 401.
(68) Pjura, P. E.; Matsumura, M.; Wozniak, J. A.; Matthews, B. W. *Biochemistry* **1990**, *29*, 2592.
(69) Weiner, S. J.; Kollman, P. A.; Case, D. A.; Singh, U. C.; Ghio, C.; Alagona, G.; Profeta, S., Jr.; Weiner, P. *J. Am. Chem. Soc.* **1984**, *106*, 765.
(70) Katz, B. A.; Kossiakoff, A. *J. Biol. Chem.* **1986**, *261*, 15480.
(71) Zhang, R.; Snyder, G. H. *J. Biol. Chem.* **1989**, *264*, 18472.
(72) van der Spoel, D.; Lindahl, E.; Hess, B.; Van Buuren, A. R.; Apol, E.; Meulenhoff, P. J.; Tieleman, D. P.; Sijbers, A. L. T. M.; Feenstra, K. A.; Van Drunenand, R.; Berendsen, H. J. C. *Gromacs User Manual*, version 3.3; Department of Biophysical Chemistry, University of Groningen: Groningen, The Netherlands, 2005; p 166, www.gromacs.org.

JP102844H